ELSEVIER

Journal of Nuclear Materials 304 (2002) 87–95

journal of nuclear materials

www.elsevier.com/locate/jnucmat

Structural features and properties of lead–iron–phosphate nuclear wasteforms

S.T. Reis [a,*], M. Karabulut [b], D.E. Day [a]

[a] *Graduate Center for Materials Research, University of Missouri-Rolla, 301 Straumanis Hall, Rolla, MO 65409-1170, USA*
[b] *Department of Physics, University of Kafkas, 36000 Kars, Turkey*

Received 4 April 2002; accepted 28 May 2002

Abstract

The structure and properties of vitreous and crystalline lead–iron–phosphate glasses containing up to 21 wt% of a simulated high level waste have been investigated using Fe-57 Mössbauer, X-ray diffraction and Raman spectroscopies. The Mössbauer spectra indicated that both Fe(II) and Fe(III) ions were present in all the samples. The Raman spectra for the glasses contained two dominant bands, which were characteristic of pyrophosphate groups, (P–O) stretching mode of P–O non-bridging oxygen at 1074 cm^{-1} and sym stretching mode of bridging oxygen at 760 cm^{-1}, respectively. The chemical durability of glassy and crystallized samples was investigated by measuring their weight loss in distilled water at 90 °C for up to 32 days. The weight loss of the lead–iron–pyrophosphate wasteforms was up to 100 times less than that for window glass. X-ray diffraction patterns showed that $FeSiO_3$ and SiP_2O_7 phases are present in samples containing more than 14 wt% of the simulated nuclear waste.

1. Introduction

Many phosphate glasses have a chemical durability which is usually inferior to that of most silicate and borosilicate glasses, but iron–phosphate glasses are an exception [1]. In addition to their generally excellent chemical durability, iron–phosphate glasses have low melting temperature, typically between 950 and 1150 °C. Investigations of iron–phosphate wasteforms obtained by adding different amounts of various simulated nuclear wastes to a base iron–phosphate glass, whose composition is $40Fe_2O_3$–$60P_2O_5$ (mol%) showed that these glassy wasteforms have a corrosion rate up to one thousand times lower than that of a comparable borosilicate glass [2–4]. Generally, iron–phosphate glasses can contain up to 40 wt% of certain simulated waste [4]. However for a lead–iron–phosphate glass with an O/P molar ratio of 3.7 [5], that contains a mixture of pyrophosphate and orthophosphate groups, the waste loading was limited to about 10 wt% [5,6].

The family of phosphate glasses with an O/P ratio of 3.5 are based on pyrophosphate (P_2O_7) groups and these glasses are chemically more stable in aqueous solutions compared to phosphate glasses with an O/P ratio different of 3.5. Because of their unusually high chemical durability and other properties, iron–phosphate glasses [2] and zinc–iron–phosphate glasses [7] are of interest for nuclear waste immobilization. Some of the high level nuclear wastes at Hanford, such as the waste from tank B-110 [8] contain high percentages of Bi_2O_3 (25.8 wt%), Fe_2O_3 (30.6 wt%) and along with other oxides such as silica, soda and alumina. The B-110 waste comes from different steps in the bismuth phosphate process which accounts for the high concentration of Bi_2O_3 [8]. Vitrifying these types of wastes in iron–phosphate glasses offers the advantage that the waste provides a considerable amount of the components (Fe_2O_3, P_2O_5) needed for glass formation, thereby, decreasing the volume of the final waste product.

* Corresponding author. Tel.: +1-573 341 4359; fax: +1-573 341 2071.
E-mail address: reis@umr.edu (S.T. Reis).

0022-3115/02/$ - see front matter © 2002 Published by Elsevier Science B.V.
PII: S0022-3115(02)00904-2

In the present study, a lead–iron–phosphate glass with an O/P ratio of 3.5, which is called lead–iron–pyrophosphate, and its wasteforms have been investigated. The objective was to investigate the chemical durability of lead–iron–pyrophosphate wasteforms (both glassy and crystalline) as a function of their composition and relate this property to the structure of the wasteforms which was studied using Mössbauer and Raman scattering spectroscopies, X-ray diffraction (XRD), and differential thermal analysis (DTA).

2. Experimental

2.1. Preparation and melting of wasteforms

Table 1 gives the composition and the raw materials used to prepare the simulated B-110 nuclear waste. The nominal batch compositions and some of the properties of simulated lead–iron–pyrophosphate samples are given in Table 2.

To obtain the maximum waste loading, the Fe_2O_3 and the P_2O_5 contents were varied, depending upon the Bi_2O_3 and the Fe_2O_3 content of the simulated nuclear waste. The simulated nuclear waste content varied from 0 to 21 wt%. The samples were melted between 1100 and 1350 °C for 2 h in air in high purity alumina crucibles. The melt was quenched in air by pouring it into a $1 \times 1 \times 5$ cm^3 steel mold. The samples were transferred to a furnace and annealed at 450 °C for 3 h.

2.2. Density, XRD and DTA

The density of the glass was measured at room temperature by the Archimedes method using water as the buoyancy liquid. The estimated error is ± 0.02 g/cm^3. The DTA measurements were performed in flowing nitrogen at a heating rate of 10 °C/min using a Perkins Elmer instrument. The samples were crystallized by heat treating at 640, 650 and 670 °C for 24 h in air. For the crystallization treatment, the temperatures of the crystallization peaks (T_c) determined from the DTA patterns were used. The estimated error in glass transition temperature (T_g) and T_c is ± 2 °C. Room temperature XRD patterns for both glass and crystalline counterparts were collected using an X-ray diffractometer (Scintag XDS2000).

Table 1
Simplified composition, wt%, of Hanford B-110 waste and raw materials used to prepare simulated B-110 waste

Compound	B-110 (wt%)	Raw materials used
Fe_2O_3	30.6	Fe_2O_3
P_2O_5	1.7	$NH_4H_2PO_4$
Bi_2O_3	25.8	Bi_2O_3
SiO_2	23.4	SiO_2
Na_2O	14.4	Na_2CO_3
Al_2O_3	2.7	Al_2O_3
CaO	1.5	$CaCO_3$

2.3. Chemical durability tests

The chemical durability of glassy and crystallized samples was evaluated from the weight loss of samples ($1 \times 1 \times 1$ cm^3) immersed in distilled water at 90 °C for 2–32 days. The samples were polished to a 600 grit finish with SiC paper, cleaned with acetone and suspended in glass flasks containing 100 ml of distilled water at 90 °C. Duplicate measurements were made for each glass and the average dissolution rate (D_R), normalized to the surface area and the corrosion time, was calculated from the weight loss.

2.4. Mössbauer and Raman spectra

The Mössbauer spectra were measured at room temperature on a spectrometer (ASA 600) which utilized a room temperature 50 mCi cobalt-57 source embedded in a rhodium matrix. The spectrometer was calibrated at 23 °C with α-iron foil and the line width of the α-iron spectrum was 0.27 mm/s. Mössbauer absorbers of approximate thickness 140 mg/cm^2 were prepared using 125 μm powders. The Mössbauer spectra were fit with broadened paramagnetic Lorentzian doublets. The Raman spectrum of each glass was measured at room temperature using a Renishaw Raman 3000 system, coupled to an Olympus metallurgical microscope. The spectra were recorded over the 200–1800 cm^{-1} range using a 632.8 nm (He–Ne laser, Spectra Physics mod. 127) source.

3. Results

3.1. XRD, DTA and density measurements

The compositions containing <16 wt% of the simulated B-110 nuclear waste (Table 2) formed glass as no crystalline phase was detected by XRD. The cast and annealed samples A7, A8 and A9, which contains more than 16.5 wt% waste content, were partially crystallized and contained $NaFeP_2O_7$ and SiP_2O_7 phases. In general, the compositions with an O/P ratio <4.2 tended to form glass. The glass-forming tendency decreased with the increasing O/P ratio, see Fig. 1. There is some uncertainty in the O/P ratio values since they were calculated from the starting batch. It is known [9–11] that the glass composition changes during melting in air since about

Table 2
Batch composition in wt% and properties of lead–iron–phosphate wasteforms containing simulated B-110 waste

Glass composition (wt%)	A0[a]	A1	A2	A3	A4	A5	A6	A7	A8	A9
P_2O_5	34.0	32.5	31.3	30.9	30.6	30.2	29.4	28.7	27.9	27.1
Fe_2O_3	12.2	13.1	13.7	13.9	14.2	14.4	14.8	15.2	15.7	16.1
PbO	53.8	51.3	49.3	48.7	48.1	47.4	46.2	44.9	43.6	42.4
Bi_2O_3	–	1.2	2.1	2.4	2.7	3.1	3.7	4.3	4.9	5.5
SiO_2	–	1.1	1.9	2.2	2.5	2.8	3.3	3.9	4.4	5.0
Na_2O	–	0.7	1.2	1.4	1.5	1.7	2.0	2.4	2.7	3.1
Al_2O_3	–	0.1	0.2	0.3	0.3	0.3	0.4	0.5	0.5	0.6
CaO	–	0.1	0.1	0.1	0.2	0.2	0.2	0.3	0.3	0.3
Waste loading (wt%)	None	4.7	8.3	9.5	10.6	11.8	14.3	16.5	18.9	21.2
Properties										
O/P ratio[b]	3.5	3.7	3.8	3.9	3.9	4.0	4.1	4.2	4.4	4.5
(Fe + Pb)/P ratio[b]	0.83	0.86	0.89	0.90	0.91	0.92	0.95	0.97	1.00	1.03
D_{RG}[c] (g/cm^2/min)	1.7×10^{-9}	1.4×10^{-9}	1.8×10^{-9}	6.2×10^{-10}	8.1×10^{-10}	3.0×10^{-9}	1.8×10^{-9}	3.6×10^{-9}	5.9×10^{-9}	4.1×10^{-9}
D_{RC}[c] (g/cm^2/min)	2.8×10^{-9}	1.0×10^{-9}	1.6×10^{-9}	7.6×10^{-10}	1.1×10^{-8}	1.2×10^{-7}	4.0×10^{-7}	nm	nm	nm
ρ (g/cm^3) ($\pm$0.02)	4.1	4.4	4.5	4.8	4.7	4.6	4.6	4.4	4.3	4.2
T_g (°C) ($\pm$2 °C)	498	nm	516	519	508	486	507	504	503	474
T_c (°C) ($\pm$2 °C)	596	nm	631	617	611	593	644	632	618	599

nm = Not measured.

[a] Starting lead–iron–phosphate glass.

[b] Molar O/P and (Fe + Pb)/P molar ratio were calculated from the batch compositions.

[c] Dissolution rates for glass (D_{RG}) and crystalline (D_{RC}) samples was measured from the weight loss experiments in distilled water at 90 °C for 32 days.

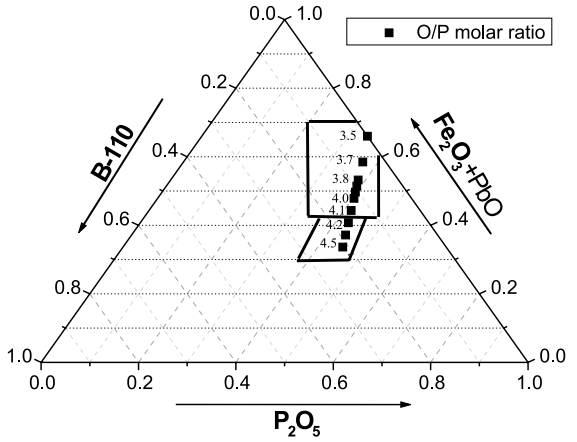

Fig. 1. General composition of lead–iron–pyrophosphate glasses containing the B-110 simulated nuclear waste are contained within the large rectangle. The small rectangle include compositions that crystallized.

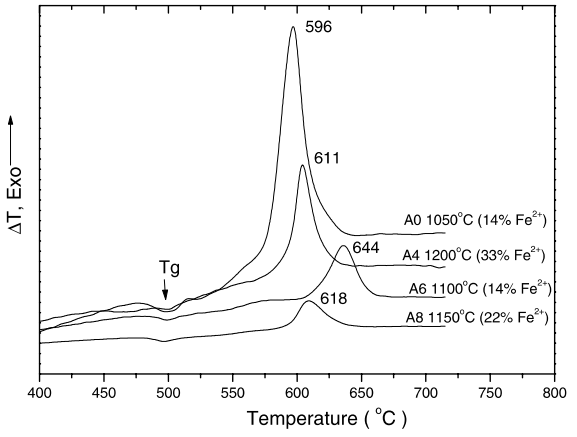

Fig. 2. DTA curves for samples with simulated waste content of 0 (sample A0) to 19 wt% (sample A8).

25% of the Fe^{3+} ions in the Fe_2O_3 raw material are reduced to Fe^{2+}, thereby, releasing oxygen.

Fig. 2 shows the DTA patterns for the base glass (A0) and glasses containing 11 wt% (A4), 14 wt% (A6), and the partially crystallized sample with 19 wt% (A8) of the simulated B-110 nuclear waste. Samples A1, A2, A3, A5 and A9 are not shown. As shown by the small endothermic peaks in Fig. 2, the glass transition temperature, T_g, for the glasses is close and ranges between 498 and 508 °C. The larger exothermic peaks at ~596, 611, 644 and 618 °C in Fig. 2 are due to crystallization of the pyrophosphate wasteforms and occur for the A0, A4, A6 and A8, respectively. Similar exothermic peaks attributed to the crystallization of $Fe_3(P_2O_7)_2$ [12] were observed between 590 and 650 °C in the DTA pattern of a $40Fe_2O_3$–$60P_2O_5$ (mol%) iron–phosphate glass melted at different temperatures.

Small portions of samples A0, A2, A4, A6 and A8 were crystallized by heat treating for 24 h in air at 600, 631, 611, 644 and 618 °C, respectively, which corresponds to the temperature of the exothermic peak in the DTA pattern, see Fig. 2, of the respective samples. The XRD patterns in Fig. 3 show that $Fe_2Pb(P_2O_7)_2$ [12] and $Fe_3(P_2O_7)_2$ [13] are the main phases present in samples containing <14 wt% of the simulated B-110 nuclear waste. As the waste content increased, the lead–iron–pyrophosphate phase ($Fe_2Pb(P_2O_7)_2$) decreased and crystalline $NaFeP_2O_7$ [14] and SiP_2O_7 [15] became dominant in the XRD spectra. The presence of the crystalline ferrous–ferric pyrophosphate ($Fe_3(P_2O_7)_2$) in all of the samples is related to the higher concentration of Fe_2O_3 and P_2O_5 in these compositions.

The density of the glass samples with waste content between 0 wt% (A0) and 10 wt% (A3) increases from 4.1 to 4.8 g/cm^3 with increasing Fe_2O_3 content (Table 2). This increase may be due to the presence of the Pb^{2+} and Fe^{3+}, which increases the cross-link density in the glass. The glass forming tendency of the compositions with high Bi_2O_3, Na_2O and SiO_2 contents decreased and these samples partially crystallized during cooling. This crystallization is related to the increase in the molar O/P ratio in these samples.

3.2. Chemical durability

The dissolution rates of the glassy (D_{RG}) and partially crystallized (D_{RC}) samples, measured from their weight loss in distilled water at 90 °C, are given in Table 2 and Fig. 4. For glasses with a simulated B-110 waste content <8 wt%, the dissolution rate is approximately constant for a given immersion time. The D_R of the glasses with simulated nuclear waste contents between 8 and 12 wt% was the smallest for the samples studied. The O/P and (Fe + Pb)/P ratios of these glasses were ~3.9 and ~0.9, respectively, which are important to chemical durability of phosphate glasses [7,17,18]. The D_R gradually increased for samples as the waste content above 14 wt%. These samples were partially crystallized and had (Fe + Pb)/P molar ratio of ~1.0. Glasses with (Fe + Pb)/P ratio of ~0.90 had a D_R value 100 times less than the D_R for window glass and comparable to the D_R of a glassy iron–phosphate (lead-free) wasteforms with a simulated B-110 waste content of 35 wt% [8]. In general, the D_R increased with increasing of waste content, however, most of the samples still had a D_R similar to window glass.

Fig. 5 and Table 2 show that the $\log D_R$ (32 days) of these glasses tends to decrease slightly with increasing O/P ratio and increasing (Fe + Pb)/P ratios. The original Fe/P ratio of the batch composition was assumed to remain constant in the glass. The D_R values for the

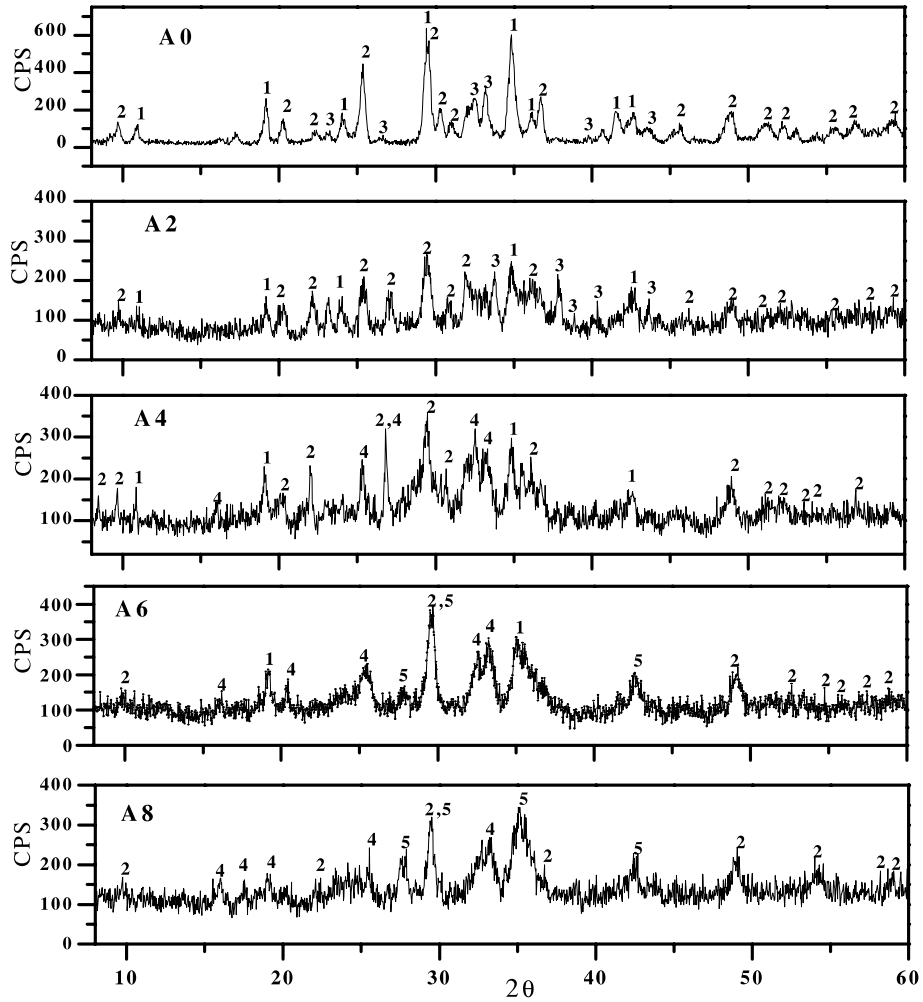

Fig. 3. XRD pattern for samples after crystallization treatment between 600 and 644 °C for 24 h in air. Crystallized phases identified by XRD were #1 = $Fe_2Pb(P_2O_7)_2$, #2 = $Fe_3(P_2O_7)_2$, #3 = $Pb_2P_2O_7$, #4 = $NaFeP_2O_7$, and #5 = SiP_2O_7.

crystallized counterparts of some of the glasses are also shown in Fig. 5. The glass and its crystalline counterpart containing <10 wt% simulated waste, see Fig. 5, had essentially identical D_R values indicating that the $Fe_2Pb(P_2O_7)_2$ phase does not adversely affect the chemical durability. For the crystallized samples whose O/P ratio exceeds ~3.9, the D_R increases with increasing simulated waste content, probably due to the formation of $NaFeP_2O_7$ and SiP_2O_7 which may have an adverse effect on the chemical durability.

There was no detectable difference in the visual appearance of the glassy samples immersed in distilled water after 32 days at 90 °C, but the external surfaces of their partially crystallized counterparts were rough and discolored. The external surfaces of samples A8 and A9, which had the highest waste contend, were discolored and lost their original sharpness.

3.3. Raman spectra

The Raman spectra shown in Fig. 6 for the glassy and partially crystallized samples include two dominant bands. These bands are characteristic of pyrophosphate groups: the bands at 1074 and 760 cm^{-1} are attributed to (P–O) symmetric stretching mode of non-bridging oxygen (NBO) and (P–O–P) sym stretching mode of bridging oxygen (BO), respectively [12,16]. There are also some traces of orthophosphate groups as indicated by the band at 924 cm^{-1} [16]. The origin of the band barely perceptible at 824 cm^{-1} remains unknown.

With increasing waste content, the bands related to the pyrophosphate groups shift from 1074 to 1090 cm^{-1} which is related to the increasing Fe_2O_3 content in the glass. This suggests an increase of the (P–O) NBOs associated with iron ions in the pyrophosphate structure.

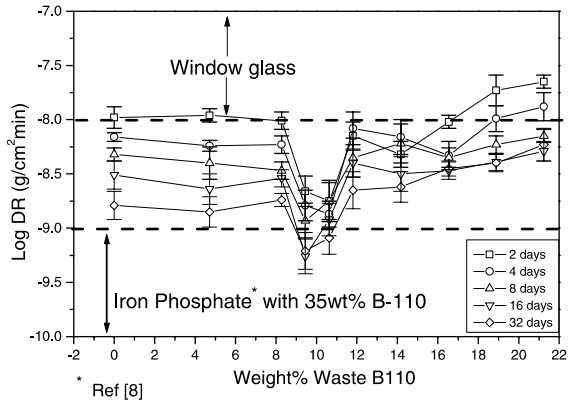

Fig. 4. Dissolution rates for glassy and partially crystallize samples, as a function of B-1110 content after immersion in distilled water at 90 °C for 2, 4, 8, 16 and 32 days. Dissolution rate for a glassy iron–phosphate wasteform containing 35 wt% B-110 waste (Ref. [8]) is shown for comparison.

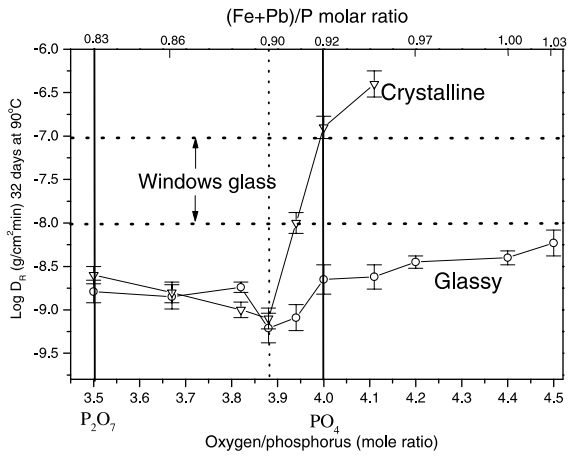

Fig. 5. Dependence of dissolution rate (32 days) of lead–iron–phosphate glassy (D_{RG}) and crystallized (D_{RC}) samples on the O/P and (Fe + Pb) molar ratios.

With increase waste content, the bands characteristic of the orthophosphate $(PO_4)^{3-}$ and metaphosphate $(PO_3)^-$ species increased. The band at 630 cm^{-1} is related to the BO (P–O–P) in metaphosphate chains [16]. However, bands at 450, 505 and 560 cm^{-1} may also be associated with silica in the glass [16]. Silica has several polymorphs with a three-dimensional silicate network. Each of these crystalline forms is characterized by bands at different frequencies in Raman spectrum for the partially crystalline sample A9.

3.4. Mössbauer spectra

The room temperature Mössbauer spectra of the lead–iron phosphate wasteforms are shown in Fig. 7.

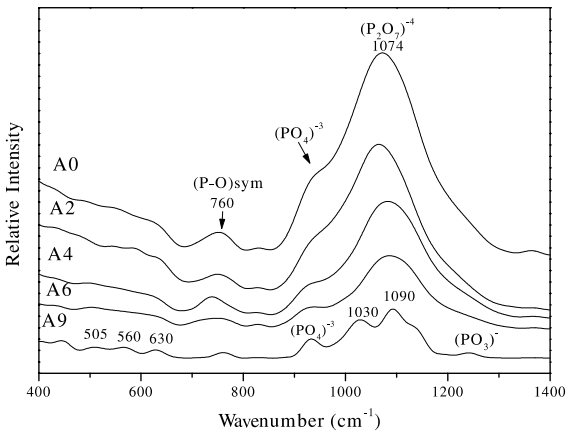

Fig. 6. Raman spectra of lead–iron–phosphate glassy (Curves A0, A2, A4) and partially crystallized (Curves A6, A9) samples.

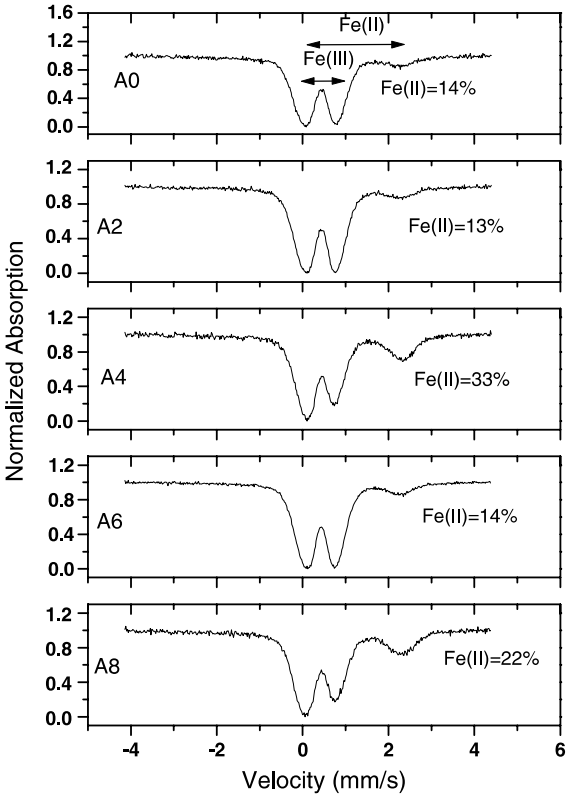

Fig. 7. Room temperature Mössbauer spectra for lead–iron–phosphate glassy and partially crystallized samples melted in air at 1050 °C (sample #A0), 1050 °C (sample #A2), 1200 °C (sample #A4), 1100 °C (sample #A6) and 1150 °C (sample #A8), respectively, for 2 h. Percent of Fe(II) and Fe(III) is shown for each curve.

The iron valence and hyperfine parameters, isomer shift δ and quadrupole splitting ΔE_Q, calculated from the

Table 3
Room temperature Mössbauer hyperfine parameters, isomer shifts $\langle\delta\rangle$, quadrupole splitting $\langle\Delta E_Q\rangle$, fraction of Fe (II) and melting temperatures for lead–iron–phosphate wasteforms

Glass	$\langle\delta\rangle$ (mm/s)		$\langle\Delta E_Q\rangle$ (mm/s)		Fraction[a] of Fe(II) (%)	Melting temperature (°C)
	Fe(II)	Fe(III)	Fe(II)	Fe(III)	Fe(II)	
A0	1.19	0.41	2.16	0.81	14	1050
A1	1.20	0.40	2.12	0.75	13	1050
A2	1.11	0.43	2.35	0.76	13	1050
A3	1.13	0.43	2.35	0.76	19	1100
A4	1.26	0.40	2.11	0.76	33	1200
A5	1.23	0.42	2.13	0.71	15	1100
A6	1.13	0.43	2.31	0.74	14	1100
A7	1.123	0.43	2.38	0.70	12	1050
A8	1.21	0.41	2.18	0.78	22	1150
A9	1.23	0.42	2.13	0.82	49	1300

The estimated error in $\langle\delta\rangle$ and $\langle\Delta E_Q\rangle$ is ± 0.03 mm/s.
[a] Fe(II)/[Fe(II) + Fe(III)] was calculated from the Mössbauer spectra.

Mössbauer spectra are given in Table 3. Some of the Fe(III) ions in the starting batch are reduced to Fe(II) ions during melting in air as the Mössbauer spectra indicate that all the glasses contain from 12% to 49% Fe(II). The higher Fe(II) concentrations in samples A4 (33%) and A9 (49%) are attributed to the higher melting temperature. In general, the concentration of Fe(II) ions increases with increasing melting temperature even when the starting batch contains only Fe(III) as Fe_2O_3 [12,19]. The isomer shift for Fe(II) and Fe(III) ions ranges from 1.11 to 1.26 mm/s and from 0.40 to 0.43 mm/s, respectively, while the quadrupole splitting ranges from 2.11 to 2.38 mm/s and from 0.71 to 0.82 mm/s, respectively. These values for the isomer shift correspond to octahedral or distorted octahedral coordination for both Fe(II) and Fe(III) ions in these glasses [19].

4. Discussion

The most extensive use of phosphate glasses for vitrifying nuclear wastes has occurred in the former Soviet Union [20], where several hundred tons of nuclear waste has been immobilized in a sodium aluminophosphate glass. Lead–iron–phosphate glasses have also been investigated in Brazil [5] for vitrifying nuclear waste, but have not been used in actual practice.

The phosphate glasses studied in the present work have properties that are significantly different from the traditional phosphate glasses such as those investigated for cesium immobilization in sintered lead–iron–phosphate glass [21].

The dissolution rate for the glasses with waste contents between 8 and 12 wt% is more than 10 times less than that of window glass, and approaches that of the $40Fe_2O_3 \cdot 60P_2O_5$ glass (see Fig. 6) which has an extremely low D_R. The maximum waste loading in the lead–iron–phosphate glasses studied for Cs immobilization was 6%, while the dissolution rate of these glasses was 10 times less than the window glass [21]. A dissolution rate of 10^{-9} g/cm^2/min measured in deionized water at 90 °C for glasses containing <8 wt% simulated B-110 waste is comparable to soda lime and borosilicate glasses. For waste loading below 10 wt%, the D_R for glassy and crystalline wasteforms was essentially identical (within experimental error). This indicates that the chemical durability of the crystalline $Fe_2Pb(P_2O_7)_2$, and $Pb_2P_2O_7$ phases in these samples is as good as that of the glass.

All of the measured properties indicate that the lead–iron–phosphorus–oxygen network becomes stronger in compositions with an O/P ratio ~3.9 and (Fe + Pb)/P ratio ~0.90. The improvement in chemical durability and increase in density are consistent with stronger bonding in the glass.

A zinc–iron–phosphate glass [7] with an O/P ratio of 3.4, whose composition is closer to the pyrophosphate composition had excellent chemical durability with a D_R of 1.3×10^{-9} g/cm^2/min at 90 °C. The O/P ratio of the lead–iron–phosphate wasteforms with simulated waste content of 9.5% in this study is 3.9. This composition, which contains pyrophosphate (P_2O_7) and orthophosphate groups (isolated PO_4 tetrahedra) has a chemical durability comparable to many other iron–phosphate nuclear wasteforms [4,12]. However, crystallized samples with higher waste contents whose XRD patterns showed $NaFeP_2O_7$ and SiP_2O_7 phases had the lowest chemical durability.

The structure of crystalline, $Fe_2Pb(P_2O_7)_2$, present in crystallized samples consists of $(Fe_3O_{12})^{16-}$ clusters where the Fe(II) ions in trigonal prism coordination are sandwiched between two Fe(III) ions in octahedral

coordination which are connected by $(P_2O_7)^{4-}$ groups [22]. This structure is very similar to that for $Fe_3(P_2O_7)_2$ which also contains $(Fe_3O_{12})^{16-}$ clusters bonded together by pyrophosphate (P_2O_7) group. Assuming general similarities between the glass and the crystal structure, the glass could contain isolated PO_4 group interconnected by Fe–O and, individual pyrophosphate groups bonded together by the Fe–O and Pb–O groups. This is consistent with the chemical durability for the glassy and crystalline pyrophosphate wasteforms.

The Raman spectra of the lead iron–phosphate wasteforms is dominated by absorptions between 1073 and 1090 cm^{-1} (Fig. 4) which are due to pyrophosphate $(P_2O_7)^{4-}$ groups. However, the phosphate network also contains some metaphosphate $(PO_3)^-$ and orthophosphate $(PO_4)^{-3}$ anion groups. In general, there is no significant difference among the Raman spectra of the lead–iron–phosphate glass wasteforms suggesting that the structure of these glasses does not change much for waste contents <16 wt%. For the partially crystallized wasteforms with waste contents up to 16 wt%, the bands at 450, 505 and 560 cm^{-1} can be associated with crystalline SiO_2.

The Mössbauer spectra indicate that the oxygen coordination of both Fe(II) and Fe(III) ions are independent of the melting conditions and waste loading. Both Fe(II) and Fe(III) ions occupy sites of octahedral or distorted octahedral coordination. Although their oxygens coordination does not change, the fraction of Fe(II) varied from 12% to 49%, especially for samples A7 and A9. In a previous study of iron–phosphate glasses, the Fe(II) fraction was found to increase with melting temperature [19]. However, this increase did not adversely affect the chemical durability indicating that both Fe(II) and Fe(III) ions played equally important structural roles which is similar to the findings of this study.

5. Conclusions

The dissolution rate for the lead–iron–phosphate wasteforms with waste contents between 8 and 12 wt% is comparable to that for $40Fe_2O_3 \cdot 60P_2O_5$ glass. The similar D_R values for glasses and their crystalline counterparts with simulated waste content below 10 wt% indicate that the $Fe_2Pb(P_2O_7)_2$ phase is important for improved the chemical durability of both glass and crystalline samples. All of the measured properties indicate that the lead–iron–phosphorus–oxygen network becomes stronger in compositions with an O/P and (Fe + Pb)/P ratios of ~3.9 and ~0.9, respectively. The XRD results indicate a structure based on $Fe_2Pb(P_2O_7)_2$, and $Fe_3(P_2O_7)_2$ pyrophosphates.

The Raman spectra are dominated by the $(P_2O_7)^-$ groups that account for absorption between 1073 and 1090 cm^{-1} which indicate that the structure of the lead–iron–phosphate wasteforms is based on pyrophosphate groups. The Raman spectra of all the lead–iron–phosphate glass wasteforms is essentially the same which suggests that the P–O network is not affected for waste contents <16 wt%. For the partially crystallized wasteforms, where the waste content is more than 16 wt%, the new bands can be associated with the crystalline SiO_2.

The Mössbauer spectra indicate that the oxygen coordination of both Fe(II) and Fe(III) ions are independent of the melting conditions and waste loading. Both Fe(II) and Fe(III) ions occupy sites of octahedral or distorted octahedral coordination.

Acknowledgements

One of the authors (S.T.R.) highly appreciates the support from the University of Missouri-Rolla, which has made this work possible. The Raman spectroscopy was performed by Professor Dalva L.A. de Faria at the Chemistry Institute, Sao Paulo University, Brazil.

References

[1] G.K. Marasinghe, M. Karabulut, C.S. Ray, D.E. Day, J. Non-Cryst. Solids 263&264 (2000) 146.
[2] M. Karabulut, G.K. Marasinghe, P.G. Allen, C.H. Booth, M. Grimsditch, J. Mater. Res. 15 (2000) 1972.
[3] M.G. Mesko, D.E. Day, J. Non-Cryst. Solids 273 (1999) 27.
[4] D.E. Day, Z. Wu, C.S. Ray, P. Hrma, J. Non-Cryst. Solids 241 (1998) 1.
[5] S.T. Reis, PhD thesis, Brazilian Nuclear Energy Commission-Energy and Nuclear Research Institute, 1999.
[6] B.C. Sales, L.A. Boatner, Mater. Lett. 2 (1984) 301.
[7] S.T. Reis, M. Karabulut, D.E. Day, J. Non-Cryst. Solids 292 (2001) 150.
[8] M.G. Mesko, D.E. Day, B.C. Bunker, in: W.W. Schulz, N.J. Lombardo (Eds.), Science and Technology for Disposal of Radioactive Tank Wastes, Plenum, New York, 1998.
[9] X. Yu, D.E. Day, G.J. Long, R.K. Brow, J. Non-Cryst. Solids 215 (1997) 21.
[10] G.K. Marasinghe, M. Karabulut, C.S. Ray, D.E. Day, C.H. Booth, P.G. Allen, D.K. Shuh, Ceram. Trans. 87 (1998) 261.
[11] G.K. Marasinghe, M. Karabulut, C.S. Ray, D.E. Day, J. Non-Cryst. Solids 222 (1997) 144.
[12] X. Fang, C.S. Ray, A. Mogus-Milankovic, D.E. Day, J. Non-Cryst. Solids 283 (2001) 162.
[13] A. Goiffon, A. Dumas, J.C. Philippot, Rev. Chim. Miner. 23 (1986) 99.
[14] H. Mcmurdie et al., Powder Diffract. 1 (1986) 75.
[15] I. Chakaraborty et al., J. Solid State Chem. 68 (1987) 94.
[16] A. Mogus-Milankovic, B. Pivac, K. Furic, Phys. Chem. Glasses 38 (1997) 74.
[17] C.S. Ray, X. Fang, M. Karabulut, G.K. Marasinghe, D.E. Day, J. Non-Cryst. Solids 249 (1999) 1.

[18] G.K. Marasinghe, M. Karabulut, C.S. Ray, D.E. Day, C.H. Booth, P.G. Allen, D.K. Shuh, Ceram. Trans. 87 (1998) 261.
[19] M. Karabulut, G.K. Marasinghe, C.S. Ray, D.E. Day, O. Ozturk, G.D. Waddill, J. Non-Cryst. Solids 249 (1999) 106.
[20] A.S. Polyakov, G.B. Borisov, N.I. Moiseenko, V.I. Osnovin, E.G. Dzenkun, At. Energ. 76 (3) (1994) 183.
[21] S.T. Reis, J.R. Martinelli, J. Non-Cryst. Solids 247 (1999) 241.
[22] D. Vigo, B.O. Mysen, Phys. Chem. Miner. 12 (1985) 65.